Supplementary material for

Interface effects in molecular beam epitaxy of $SrMnSb_2$ on InAs and GaSb: segregation and endotaxy

Thomas J. Rehaag et al.

1. Structures from Materials Project

The calculated orthorhombic (Pcmn) and tetragonal (P4/nmm) unit cells of $SrMnSb_2$ are available in Materials Project, and are linked and summarised here:

mp-1208681	-0.530 eV / atom	a = 4.45, b = 4.52, c = 22.63 Å
mp-1079721	-0.529 eV / atom	a = b = 4.42, c = 11.72 Å

2. Additional XRD analysis

Figure S1 shows more detail for the XRD pattern given in the main text, Fig. 3. The detailed peak position fitting gives an out of plane lattice parameter 25.074(4) Å for the $SrMnSb_2$(001) film, with a reduced chi-squared value of 0.84. Fitting of the peak widths according to Scherrer's formula gives a grain size of 10.7 nm (reduced chi-squared 0.58), much smaller than the nominal film thickness of 80 nm.

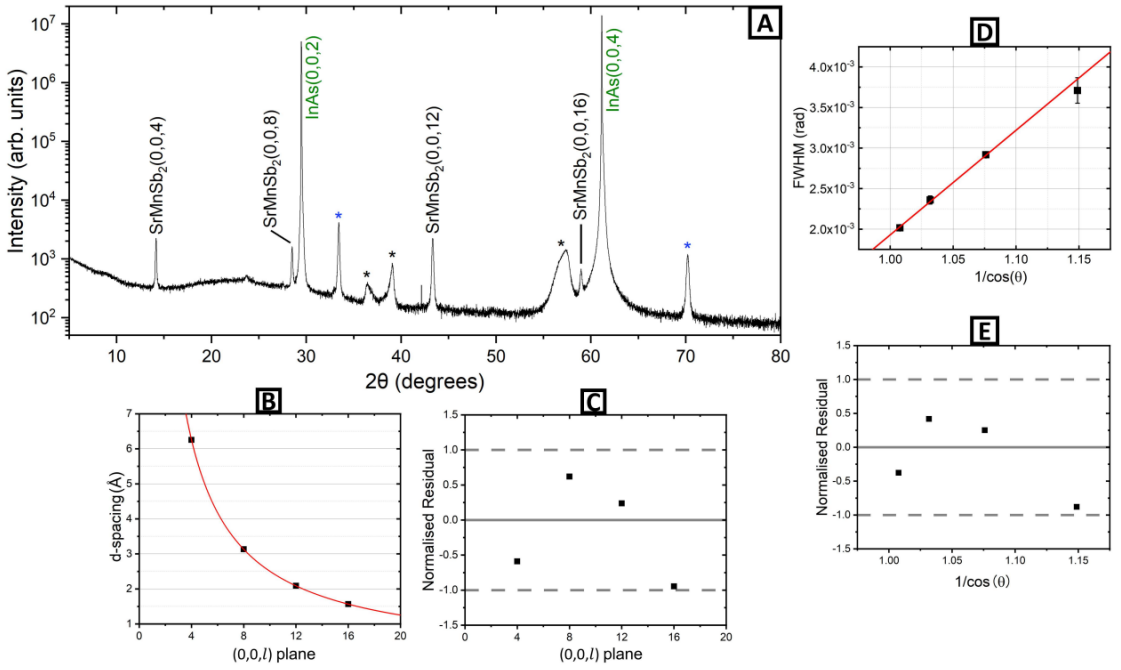

Figure S1. XRD with fitting and Scherrer analysis for 80 nm $SrMnS_2$ grown directly on InAs(001). Panel A repeats the diffractogram shown in the main text, while B and C show the fit and residuals for the out of plane lattice parameter. Panels D and E show the Scherrer fit and residuals.

3. Additional RHEED analysis

Figure S2 shows RHEED patterns for $SrMnSb_2$ grown directly on InAs(001) and a typical measurement of out of plane lattice parameter. If the starting InAs surface is rough (panel B), caused by poor chemical etching and/or excessive Ar ion sputtering, the film does not recover smoothness at any point during the growth. For a smooth starting surface (panel A), with (4×2) / c(8×2) reconstruction, the pattern gradually becomes spottier as the $SrMnSb_2$ thickness increases above ~ 20 nm. The presence of transmission diffraction (spotty "grid" pattern) allows the out of plane $SrMnSb_2$ lattice parameter to be derived. The coloured lines in Fig. S2(C) show the spacing calculation. The diagonal pattern of spots allows each family of reflections to be identified, and the coloured horizontal lines represent the out of plane spacing between them. The key point is that for all samples thus measured, the out of plane spacing is close to *c* / 2 for the bulk unit cell, i.e. around 12 Å. The out of plane expansion relative to the bulk crystal unit cell which was found in XRD is reproduced in the RHEED measurements.

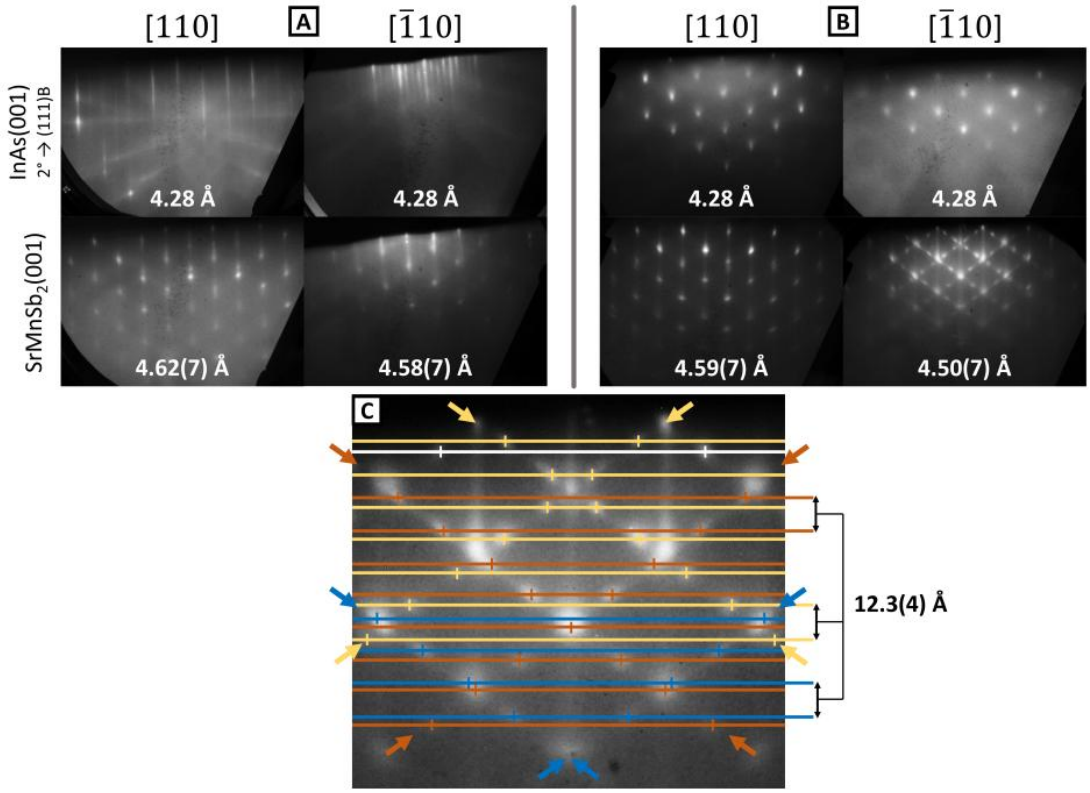

Figure S2. Comparison of RHEED patterns before and after $SrMnSb_2$/InAs(001) growth on (A) a at (4×2) reconstructed surface, and (B) a rough starting surface with measured in-plane lattice constant superimposed on each image. (C) An enlarged view of RHEED in the [-110] direction with markers placed on transmission spots between integer order streaks. Markers are colour coded such that spots along the same diagonals are in the same set, as indicated by arrows, with horizontal markers connecting equivalent spots at equal heights. Lattice directions are in reference to substrate orientation, and layers are expected to be rotated 45° with respect to the substrate.

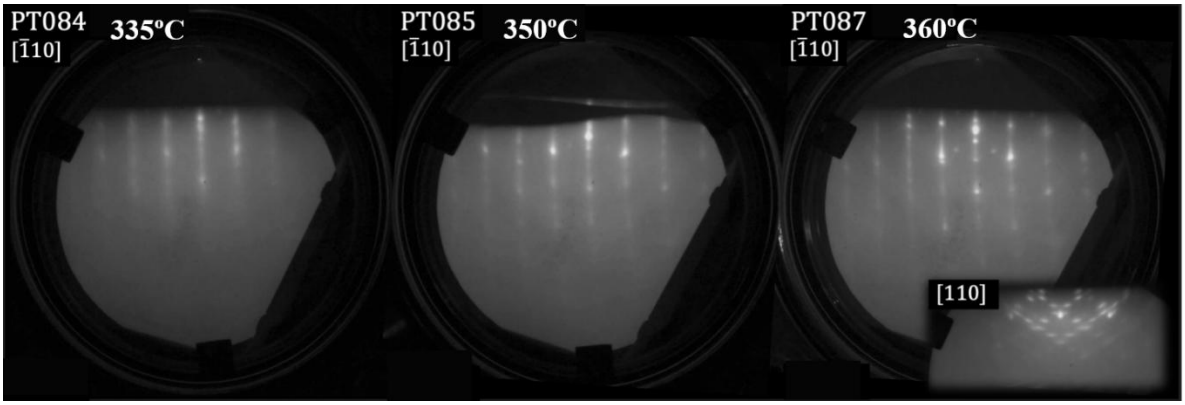

Figure S3. Comparison of RHEED patterns at different substrate temperatures for $SrMnSb_2$ / GaSb / InAs(001) growth. Substrate temperatures are shown on each pattern. An additional pattern from the perpendicular direction is shown for the highest temperature, displaying complex 3D diffraction.

Figure S3 compares RHEED patterns after 30 minutes $SrMnSb_2$ growth on GaSb / InAs(001) at different substrate temperatures. The patterns become significantly spottier at temperatures above the optimum although the background can be slightly lower and the diffraction features marginally sharper. At the highest temperatures, complicated 3D patterns combining powder diffraction-like ring structures and transmission diffraction could appear. Such samples were unrecoverable, i.e. further $SrMnSb_2$ growth never smoothed the surface and returned to streaky patterns.

Figure S4 shows in-plane lattice spacing derived from RHEED video capture at the early stages of SrMnSb2 growth on a GaSb buffer layer on InAs(001). There is no measurable change of lattice parameter for the first ML of growth: it remains close to the substrate value of ~4.3 Å. The blank region between 0.4 and 0.9 ML occurs because the RHEED pattern becomes weak and reliable extraction of streak spacing is not possible.

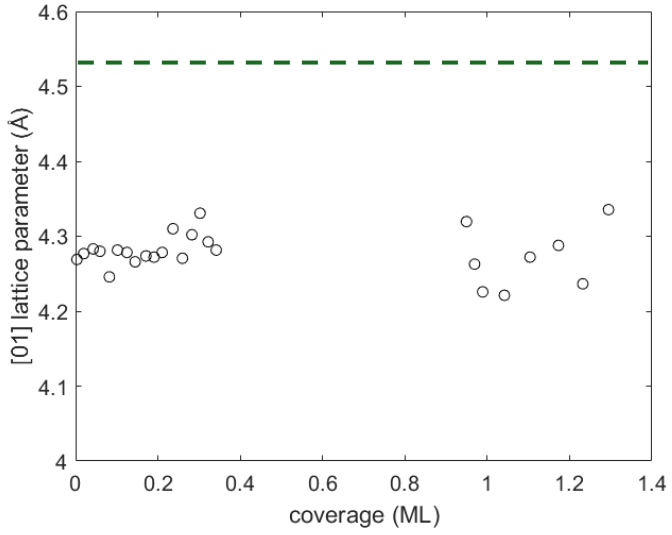

Figure S4. In-plane lattice parameter as a function of coverage at the early stage of $SrMnSb_2$ growth. The green dashed line represents the averaged (*a*,*b*) parameter of bulk SrMnSb2.

Comparing the *in-plane* RHEED lattice parameters in the orthogonal directions is key to distinguishing the tetragonal from orthorhombic $SrMnSb_2$ structures. Because we are measuring relative lattice parameters (*a* vs. *b*), provided the sample-to-screen length *L* does not change on 90º rotation, the relevant uncertainty is purely that of the streak spacing measurement. We have previously calculated the absolute error in lattice parameter at 1.6% for this MBE system based on uncertainty in *L*. The uncertainty for relative lattice parameters measured from the same sample (*a* vs. *b*) should be significantly smaller than this. The difference between bulk $SrMnSb_2$ *a* and *b* parameters is (4.46 – 4.41) / 4.41 = 1.1%, and so this should be measurable by RHEED. Because no consistent difference was observed for many $SrMnSb_2$ epilayers, it is concluded that the *a* and *b* parameters are not distinguishably different.

4. Additional TEM, STEM and EDX

Figure S5 shows low magnification STEM ADF images of samples growth without (a, b) and with (c) segregation suppression protocols (Sb soak and delayed Mn flux). In the former case, endotaxial phases appear beneath most of the interface, and strong 3D island growth is also evident (consistent with the spotty RHEED patterns). The segregation suppression protocols appear to reduce the degree of endotaxial phase formation, but it is not eliminated. Clear features, mainly triangular appear, beneath the interface extending as much as 100 nm below. For these early samples, the growth temperatures were higher than the optimised substrate temperature, at 375 ºC (no suppression) and 360 ºC (suppression) respectively. This likely enhances both the endotaxy and roughening of the $SrMnSb_2$ epilayer.

Figure S6 shows STEM images of samples grown without (A) and with (B) segregation suppression protocols (Sb soak and delayed Mn flux), at regions above endotaxial inclusions. The local EDX compositions averaged within each of the numbered yellow boxes are tabulated below. The oxygen content arises from a delay between specimen preparation and STEM measurements (minimised in subsequent experiments). The O is neglected in calculating the In % composition column of the table. The samples were capped with Sb (A) or As (B) before removal from the UHV system. Additionally sample B was subjected to ion sputtering after (without leaving UHV) after about 20 nm $SrMnSb_2$ deposition before growth was resumed.

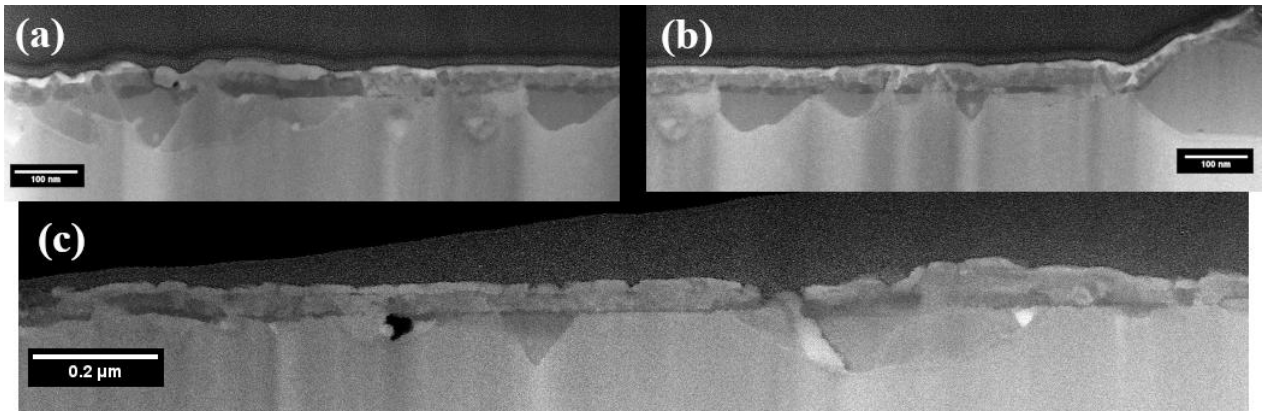

Figure S5. STEM ADF images at magnification 200,000 (a,b) and 100,000 (c) of $SrMnSb_2$ samples growth without (a,b) and with (c) segregation suppression protocols on InAs(001). Severe endotaxial phase formation is evident across most of the interface when no suppression is used (a,b). The endotaxy is much reduced in (c) but still evident as triangular or dome-shaped regions of sub-surface disruption.

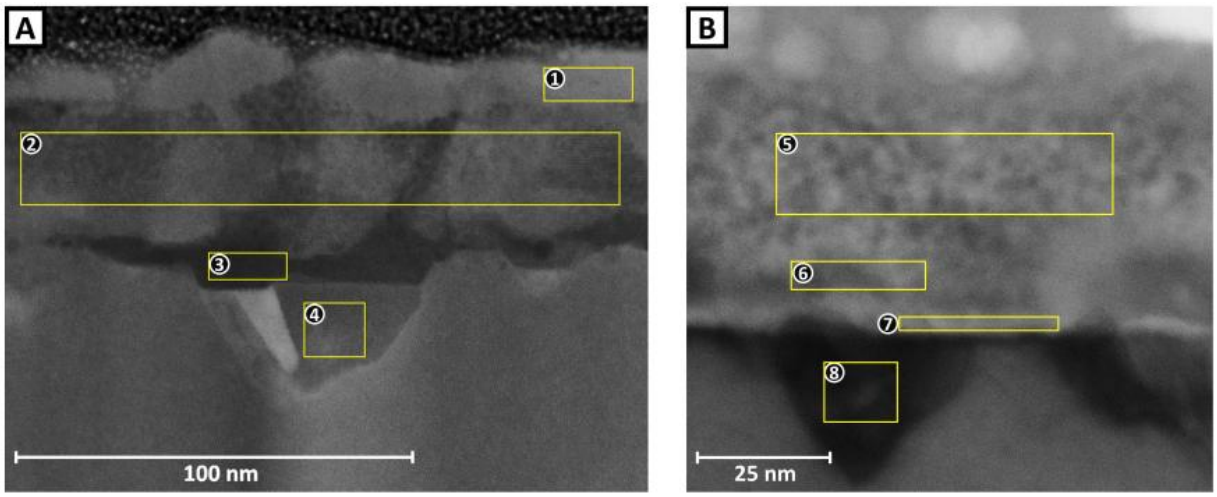

Region	Sr (%)	Mn (%)	Sb (%)	In (%)	As (%)	O (%)	In/Film (%)
1	0.0	1.6	73.3	7.8	0.7	16.6	–
2	5.9	12.1	31.6	18.3	0.6	31.5	26.7
3	8.5	28.3	1.5	1.8	25.9	34.0	2.7
4	0.0	51.0	0.8	3.0	25.1	20.1	–
5	7.7	14.3	18.0	2.7	4.6	52.7	5.7
6	6.6	13.6	14.8	7.9	4.8	52.3	16.6
7	4.5	15.4	5.2	10.5	11.2	53.2	22.4
8	1.1	34.4	2.5	14.8	36.9	10.3	–

Figure S6. ADF images in STEM for two samples of $SrMnSb_2$ on InAs(001), (A) without and (B) with segregation suppression protocols. Regions including endotaxial inclusions are shown. The numbered yellow boxes correspond to analysis regions for EDX, whose results are tabulated below.

In Fig. S5 (A), region 1 is part of the Sb cap, but it still contains segregated In. Region 2, the bulk of the $SrMnSb_2$ film, shows poor stoichiometry and a large fraction of In (similar to Sr + Mn). Region 3, close to the interface, is highly Mn rich. Region 4, within an endotaxial nano-cluster, is rich in Mn and As. These regions highlight the importance of Mn in endotaxy and support the use of delayed Mn flux in suppressing this growth mode. In Fig. S5 (B), Region 5 shows a low In fraction and Mn-enriched $SrMnSb_2$ which appear as very small grains. This region was deposited after the growth interruption and argon ion sputter. The $SrMnSb_2$ immediately below, Region 6, the also Mn-enriched but appears as much larger grains. This is consistent with RHEED, which showed only uniform intensity after the ion sputter, and weak powder-like ring patterns during annealing and subsequent $SrMnSb_2$ growth. However, the In content of region 6 is much greater, consistent with In surface segregating and being largely removed by the argon ion sputter. In enrichment is even stronger near the interface, Region 7, and the triangular endotaxial cluster (Region 8) is dominated by stoichiometric MnAs.

Another overview of $SrMnSb_2$ film growth on InAs(001) using the segregation suppression prootocols is given in **Figure S7**. Much of the interface still shows disruption. The dome-like endotaxial nano-cluster on the left has a high concentration of Mn on its right half, and the continuous intensity of As in that half suggests a MnAs inclusion. The left half of this nano-

cluster is deficient in As but contains In and Sb, suggesting endotaxial growth of InSb. A region of As segregation can be seen on the right of the image. There is a corresponding increase of Mn concentration. This lies above an endotaxial region with elevated Sb and In concentration. The appearance of InSb-rich clusters highlights the range of phases which can appear endotaxially and as a result of segregation. The granular structure of parts of the $SrMnSb_2$ film is highlighted by the ADF STEM image in **Figure S8**. This sample was grown directly on InAs(001) with Sb soak and delayed Mn flux. The rectangular symmetry of the epitaxial $SrMnSb_2$ is evident in the grains, except in the top right of the image. Two small regions of endotaxy, extending less than 10 nm into the substrate, are highlighted by yellow lines. Different grains of $SrMnSb_2$ are highlighted by unit cells (orange boxes) and show some small relative angular and lattice size distortions.

Figure S9 shows STEM-EDX data for a $SrMnSb_2$ film grown directly on GaSb(001) with Sb soak and delayed Mn flux (expanded version of the main paper Fig. 9). It is not clear how the "holes" in the As cap (centre and right of As EDX map) have arisen, but this does not affect discussion of the film and interfaces. The epilayer surface comprises flat-topped mesa-like structures, as shown by the interface between the $SrMnSb_2$ and the As cap. The lower interface is more abrupt that those seen on InAs(001), with a mostly planar and sharp transition in the Sr and Ga EDX maps. However, there are two protruding endotaxial Mn-rich regions. The region around the Ga-rich "streak" in the film is enriched in Mn and deficient in Sr. This shows how quite complicated chemical non-uniformities can occur within and below the films.

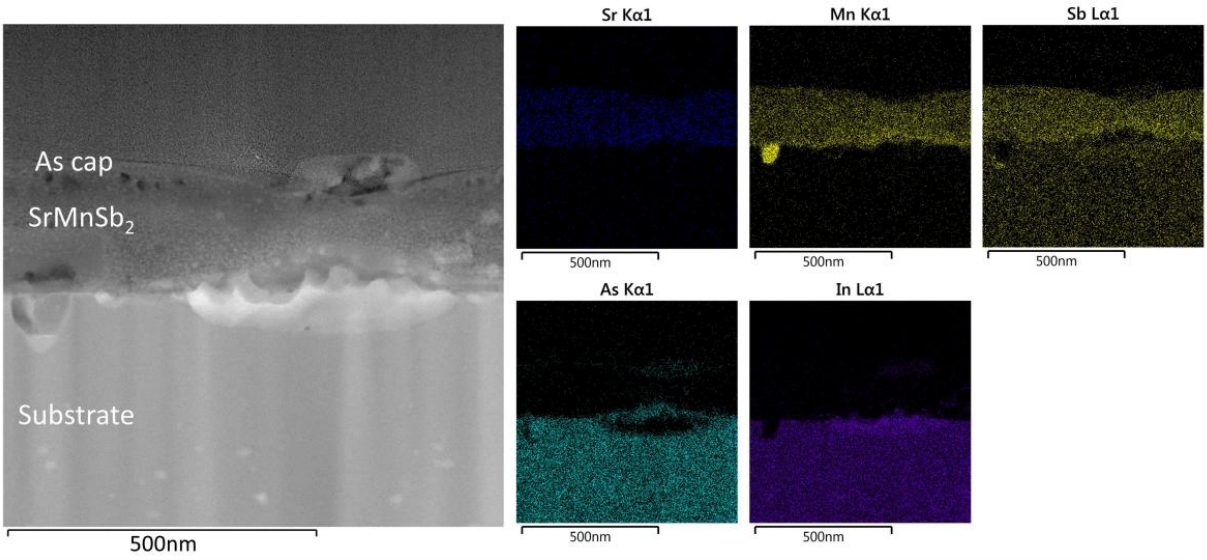

Figure S7. STEM image (left) and corresponding EDX maps (right) for a $SrMnSb_2$ film grown on InAs(001) using Sb soak and delayed Mn flux. Regions of the As-capped sample are labelled on the electron image.

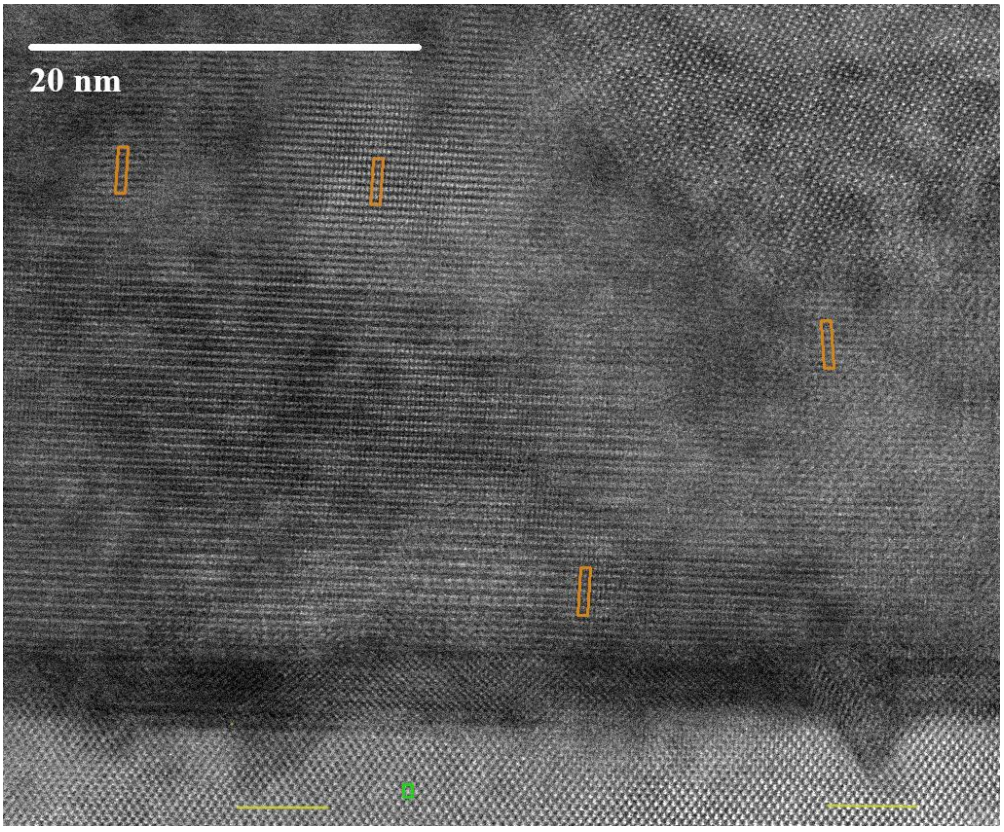

Figure S8. ADF STEM image for an epilayer of $SrMnSb_2$ grown directly on InAs(001). Small regions of endotaxy are highlighted with yellow lines. Unit cells are shown in green (InAs) and orange ($SrMnSb_2$).

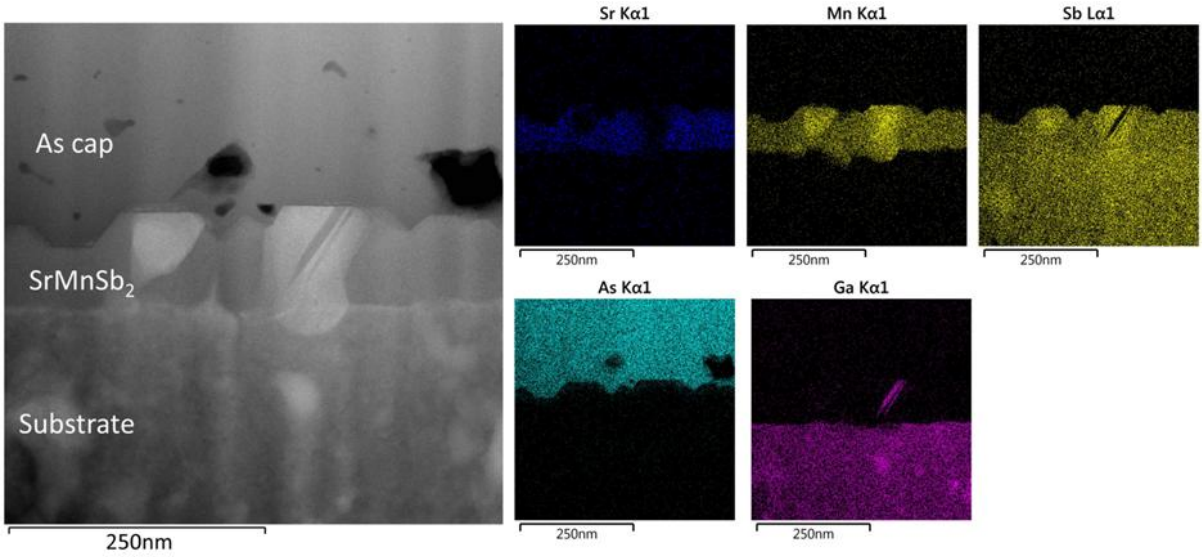

Figure S9. STEM image (left) and corresponding EDX maps (right) for a $SrMnSb_2$ film grown on GaSb(001) directly using Sb soak and delayed Mn flux. Regions of the As-capped sample are labelled on the electron image.

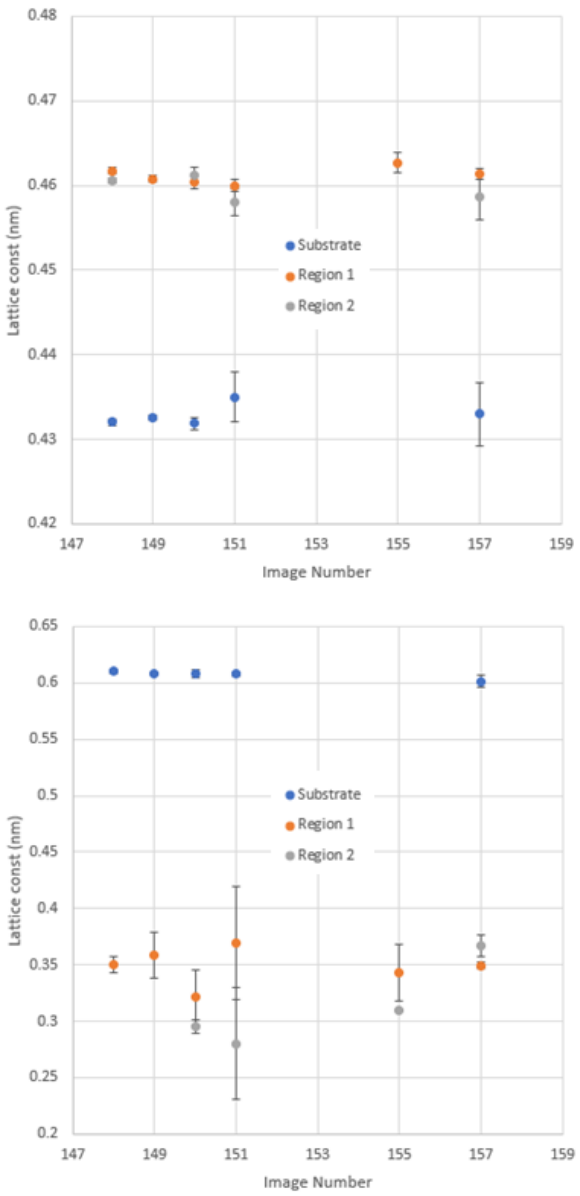

Figure S10. In plane and out-of-plane periodicities derived from several STEM images for $SrMnSb_2$ grown directly on InAs(001). Region 1 is close to the interface and Region 2 lies further into the bulk of the film.

Figure S10 shows lattice parameters derived from a series of STEM images in two regions of a sample grown directly on InAs(001). The substrate lattice parameters are as expected and show no significant variations. However, it is also clear that the film lattice parameters are quite uniform as well. Even well-ordered regions of the films are not divided into strained and relaxed regions with respect to distance from the substrate.

5. Additional XPS

Using the rule of thumb that 99.7% of the intensity derives from a depth of 3λ (λ = photoelectron inelastic mean free path) at normal exit, the effective probing depth of the XPS for the shallow core region (up to ~ 50 eV binding energy) is 6.0 nm, falling to 4.6 nm at the Mn 2p edge and 2.1 nm for As 2p.

An XPS survey scan for a $SrMnSb_2$ epilayer grown on GaSb buffer layer on InAs(001) is shown in **Figure S11**. The sample was transferred through air without As cap, and had become contaminated, hence the O and C photoelectron and Auger-Meitner features. The expected elements are present; however, the presence of indium is shown by the clear In 3d doublet. This means that In has segregated through the GaSb buffer layer into the $SrMnSb_2$ epilayer.

XPS spectra for a $SrMnSb_2$ epilayer grown on GaSb buffer layer on GaSb(001) are shown in **Figure S12**. Note that this sample had a thin GaSb overlayer grown on top of the $SrMnSb_2$ for transfer to XPS. All the peaks are fitted by a single component: no chemically shifted components are needed. However, it should be borne in mind that these data were obtained on with a non-monochromated X-ray source and a higher resolution spectrometer may reveal chemical shifts.

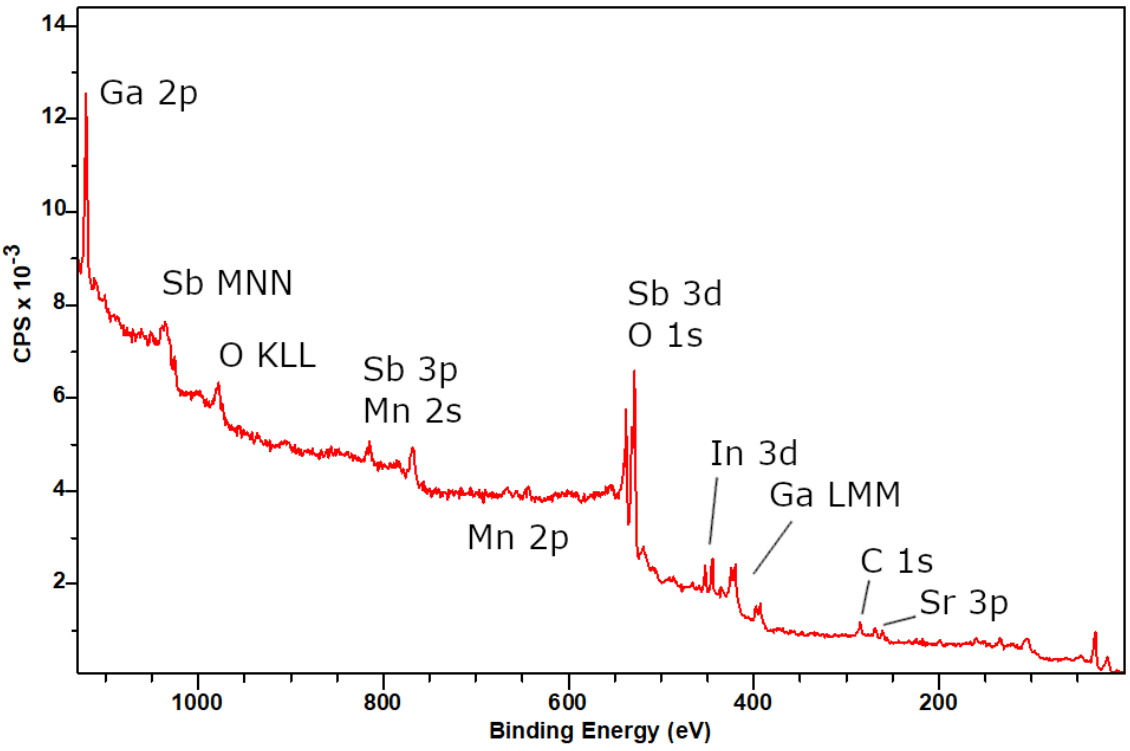

Figure S11. XPS survey scan for $SrMnSb_2$ grown on GaSb buffer layer on GaSb(001) and transferred through air without As cap. The main photoelectron and Auger-Meitner peaks are labelled.

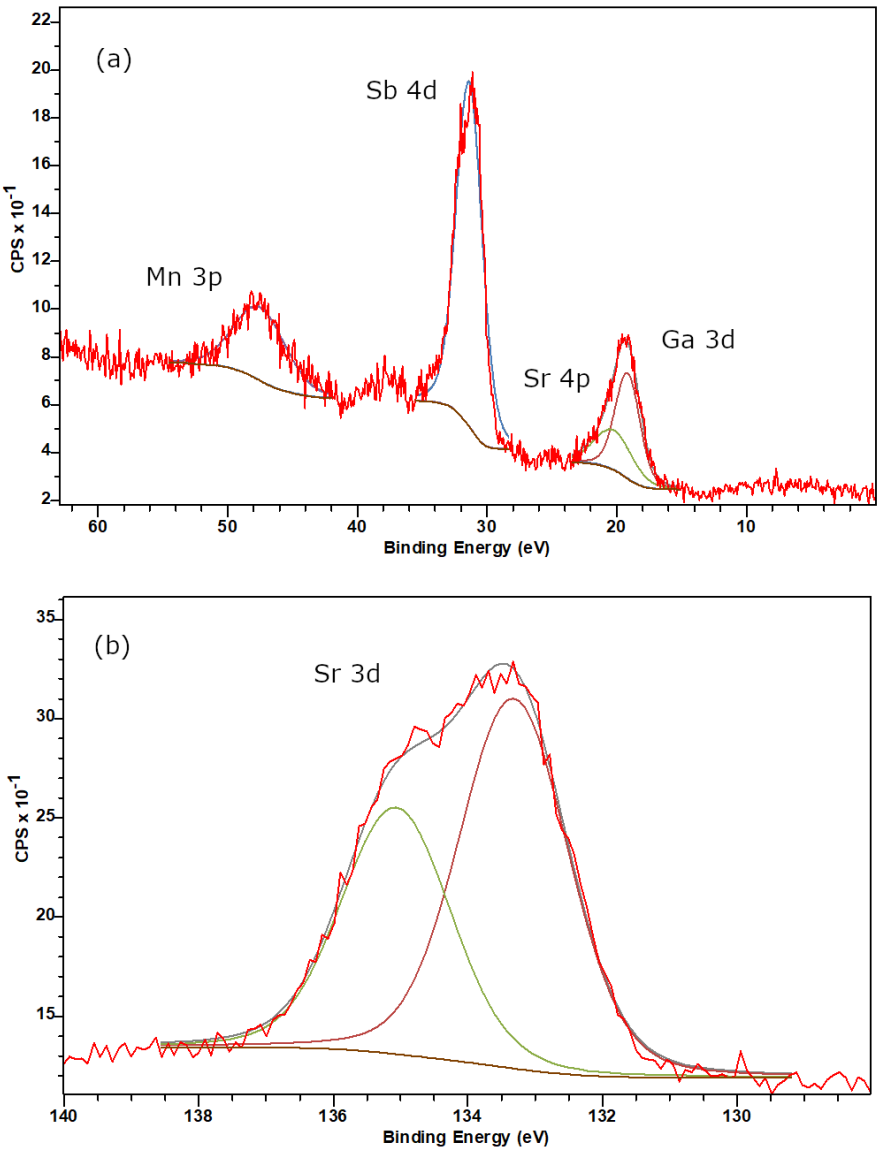

Figure S12. Shallow core (a) and Sr 3d (b) XPS data for $SrMnSb_2$ grown on GaSb buffer layer on GaSb(001). Shallow core photopeaks are fitted with single components and Shirley backgrounds, while the Sr 3d is fitted with a single spin-orbit split doublet (Δ = 1.75 eV).